Discharge Performance Analysis of different types of Gridded Ion Engines using Alternative Propellants

IEPC-2022-268

Presented at the 37th International Electric Propulsion Conference
Massachusetts Institute of Technology, Cambridge, MA USA
June 19-23, 2022

Nazareno Fazio[1], Igor O. Golosnoy[2], and Stephen B. Gabriel[3],
University of Southampton, Southampton, SO17 1BJ, United Kingdom

Abstract: Xenon is the preferred propellant for electric propulsion thrusters, providing high thruster efficiency and long life. However, xenon is very expensive and has limited availability, which could impose serious constraints on the use of electric propulsion in some future missions. This report investigates the impact of using krypton and a 1:4 Xe/Kr mixture instead of xenon on the discharge chamber performance. Calculations have been carried out for three different plasma generators using 0-D models available in literature. The results of this comparison indicate that the relative increase in total power (which is given by the increase in the discharge power and in the beam power) is around 23.5-25.5% for krypton and around 17-19% for the mixture at the selected similar operating points based on keeping similar discharge loss for the two propellants; if the operating points are chosen based on maintaining the same propellant utilisation efficiency, the increase in total power goes up to around 28-30% for krypton and around 21-22% for the mixture for the three plasma generators. Therefore, the result of the comparison shows that the three thruster configurations provide a similar behaviour and similar loss in performance when alternative propellants are used, and no plasma generators offer a clear advantage over the competing technologies.

I. Nomenclature

A_g = grid area [m^2]
A_w = wall area [m^2]
C_0 = primary electron utilization factor [A eq.$^{-1}$]
f_B = extracted-ion fraction
f_C = fraction of ion current produced that goes to cathode potential surfaces
f_{conf} = confinement factor
I_a = electron current to the discharge chamber wall [A]
I_b = beam current [A]
I_d = discharge current [A]
I_P = ion production current [A]
I_s = ion current to screen grid [A]
I_w = ion current to the discharge chamber wall [A]
I^+ = singly ionised particle production current [A]
I^{++} = doubly ionised particle production current [A]
I^* = excited neutral production current [A]
l_c = primary electron containment length [m]

[1] PhD Student, Tony Davies High Voltage Laboratory, University of Southampton, n.fazio@soton.ac.uk
[2] Associate Professor, Tony Davies High Voltage Laboratory, University of Southampton, I.Golosnoy@soton.ac.uk
[3] Professor, Tony Davies High Voltage Laboratory, University of Southampton, sbg2@soton.ac.uk

n_0 = neutral atom density [m^{-3}]
P_{abs} = power absorbed by the plasma [W]
P_d = discharge power [W]
T_e, T_{eV} = plasma electron temperature [K] or [eV]
T_s = effective grid transparency
U^+ = first ionisation potential [eV]
U^{++} = second ionisation potential [eV]
U^* = average excitation potential over the excited species [eV]
v_a = ion acoustic velocity [m/s]
v_0 = neutral atom velocity [m/s]
V_C = potential (relative to cathode) from which electrons are accelerated to become primaries [V]
V_d = discharge voltage [V]
V_P = plasma volume [m^3]
$\langle \quad \rangle$ = average over the entire electron energy distribution function, reaction rate coefficient
ϵ_0^* = average plasma ion energy cost for ionization and excitation processes only [eV]
ϵ_M = average energy of Maxwellian electrons leaving the plasma at the anode [eV]
ϵ_P^* = baseline plasma ion energy cost [eV]
η_d = ionisation efficiency or discharge loss (specific discharge power) [W/A] or [eV/ion]
η_m = thruster mass utilization efficiency
σ_0 = total inelastic collision cross section for primary electron-neutral atom collisions [m^2]
σ_i^+ = first ionization collision cross section [m^2]
σ_i^{++} = second ionization collision cross section [m^2]
σ^* = excitation collision cross section [m^2]
ϕ = potential of the plasma in the discharge chamber [eV]
ϕ_0 = grid transparency to neutral atoms

II. Introduction

The development of the GIESEPP project [1], the first European Plug and Play Gridded Ion Engine Standardised Electric Propulsion Platform, targets reducing the cost of GIE systems and increasing their production capacities. In an attempt to achieve these objectives, an investigation into the functionality and performance of the GIESEPP systems with propellants other than xenon is highly beneficial.

Xenon is the most common propellant used for space electric propulsion applications, particularly in GIEs and Hall Effect Thrusters (HETs), due to its peculiar physical and chemical properties, such as low first ionization energy, high atomic mass, and chemical inertness. However, this gas has some disadvantages, such as limited availability (and, consequently, high cost) and low density (compared to liquid and solid propellants). In particular, the former one is predicted to become more and more relevant in the future due to the increasing demand for Xe not only in the space propulsion sector, but also in many other industries (e.g., electronics, automotive, medicine, lighting, etc.). Therefore, the search for viable alternative propellants has gained momentum in the last decade because of the revival of EP technologies targeting a growing diversity of vehicles, missions, and manoeuvres.

An initial assessment [2] was carried out through a comprehensive review of the published data on the usage of alternative propellants, such as other noble gases, iodine, and other more exotic propellants (i.e., Buckminsterfullerene and Adamantane). Thereafter, a qualitative analysis was performed which looked at the impact of this range of candidates on the different GIE's systems (e.g., storage, FCU and PPU, cathode operation, plume/spacecraft interaction, toxicity, and lifetime). This was followed by a more in-depth and quantitative analysis which calculated the effects on performance. Based on these preliminary results, the best alternative within the GIESEPP project's scope would appear to be krypton if all of the selected impacts are taken into consideration; in fact, iodine has the best performance, but it was eliminated because of system compatibility issues, in addition to spacecraft contamination and toxicity.

The objective of this paper is to quantify the impact on the power supply of using alternative propellants (i.e. krypton and a Xe/Kr mixture) instead of xenon when different thruster plasma generators (i.e., DC ring-cusp, DC Kaufman, and RF) are considered. 0-D models available in literature [3–5] have been utilized to model the discharge chamber. This analysis is to evaluate the impact on the existing systems and not to address what is required to design and develop an optimised system.

The Xe/Kr mixture is considered as a possible mitigation to the problems introduced by the use of pure krypton

(i.e. loss of performance, discharge instability, and lower discharge efficiency), while, at the same time, allowing a consistent saving on the price of the propellant [6]. The storage ratio of 1:4 Xe/Kr is investigated since this is the production mixture obtained as a by-product of the separation of air into oxygen and nitrogen using conventional methods [7].

The paper is organised as follow. In Section III, the three different plasma generators and their main differences are described; in Section IV, the performance models used to evaluate the impact of using alternative propellants are introduced; in Section V, the results of the simulations are presented, including a comparison of the outcome in order to identify the technology least affected by the change of propellant; finally, general conclusion and possible perspectives are summarized in Section VI.

III. GIE Architecture: Geometry and Working Principles

A typical electric thruster can be divided in three regions based on the involved process [8] (Figure 1): the plasma source region, where the propellant is ionised to obtain plasma by transferring electrical energy to it; the ion extraction/acceleration region, where the ionised propellant is accelerated to produce thrust; the ion beam neutralisation region, where the electrically charged plasma plume is neutralised to avoid charge imbalance with the spacecraft.

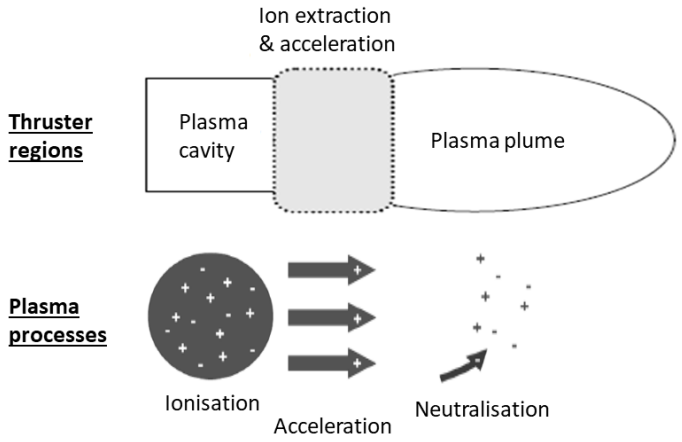

Figure 1 Schematic of the three regions and relative processes

In an ion thruster, these three basic processes are almost physically distinct with a strong coupling at the boundaries and interfaces. This is the main feature that distinguish this type of thruster from other electric thrusters, and it allows a greater control over thrust and exhaust velocity.

In this report, the focus is on the plasma generation section (discharge chamber) and on two different plasma production mechanisms amongst the several that has been tested and used in the past [9]:

- DC coupled discharge (electron bombardment)
- RF inductive discharge

In an ion thruster working in DC mode, a discharge is ignited inside the ionisation chamber where energetic primary electrons (10-50eV) impact with the propellant atoms to create ions and to generate the plasma. In order to improve the ionisation efficiency, the electrons are confined using strong magnetic field to increase the time they reside in the chamber, hence increasing the degree of ionisation. Two main variants of this configuration are considered for this study (Figure 2):

- Kaufman configuration [10] (used mostly in the UK and Russia): the cylindrical anode is isolated from the thruster body and the electrons, generated by the hollow cathode, reach this anode by cross-field diffusion. A strongly divergent magnetic field is present, and it is generated by solenoids, which require a power supply, and allows for a very fine control of the plasma density (and thrust) and a large throttleability. Further, a baffle is present at the cathode exit to flatten the plasma density profile.
- Ring cusp configuration [11] (mostly in the USA): the discharge chamber becomes the anode, and it is the cathode body that is isolated from the chamber. The magnetic field is generated by permanent magnets which give less flexibility than the Kaufman variant, but it gives a more efficient discharge (higher thrust-to-power

ratio, less thermal dissipation), and a flatter plasma profile at the grids without the need for an extra power supply for the solenoids.

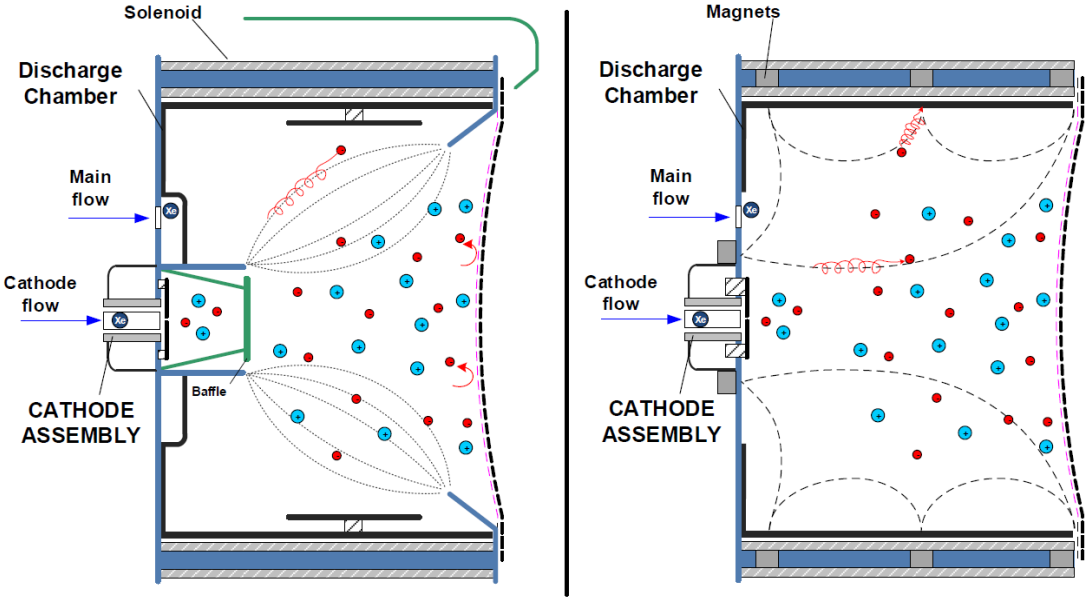

Figure 2 Kaufman configuration (on the left) vs. ring cusp configuration (on the right) [12]

On the other hand, in a GIE working in RF mode, electrons oscillating in high frequency electromagnetic fields are used to heat the plasma electrons and ionise the injected propellant [13]. This heating process is achieved using a low frequency inductive plasma generator, from here the name of radiofrequency (RF) ion thruster (Figure 3). In this configuration, an RF current (few MHz) is generated in a coiled antenna structure wrapped around the thruster body, and the electromagnetic field energy is coupled to the electrons. This RF current induces an axial magnetic field which heats the plasma electrons and maintains the ionisation process.

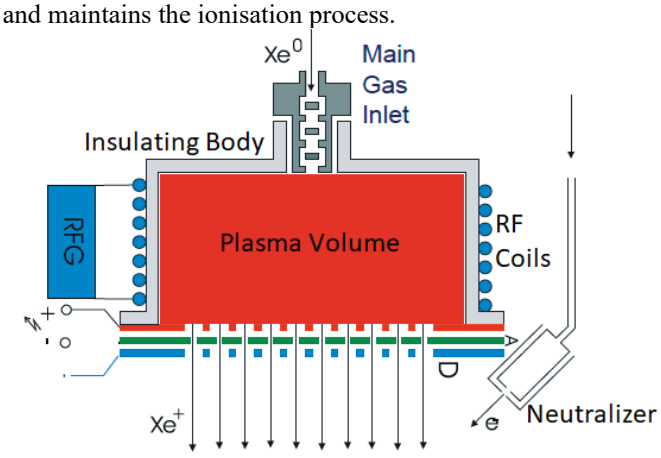

Figure 3 Schematic of a RF ion thruster [13]

RF ion thrusters have a slightly lower thrust efficiency compared to DC thrusters (~5% lower) due to higher discharge loss (mainly caused by higher ion losses to walls [5]) and to the necessity of a DC-to-RF conversion (Radio Frequency Generator, RFG). However, they offer several advantages, such as increase of lifetime (lower erosion of the chamber and absence of the internal cathode) or reduction of any potential power supply (DC-electron discharge) issues, the magnetic confinement is not necessary, lower sensitivity to impurities in the propellant (i.e. possibility to use xenon of lower purity), and higher compatibility with alternative propellants (due to the absence of the internal cathode). This kind of thruster originated and is mainly developed in Germany, and, recently, also in the USA and in the UK.

Each of these discharge chamber configuration presents a different magnetic confinement physics which needs to be addressed within the model as described in the following section.

IV. Discharge Chamber Performance Models

In order to understand and quantify the impact of using different propellants on thruster performance, it is desirable to have a model that describes the cost of producing ions in the discharge chamber. In an ion thruster, this value is usually measured in terms of the power (in watts) necessary to produce, but not accelerate, an ion beam current of 1 A at a given propellant utilization efficiency. This power is defined by an ion production term

$$\eta_d = \frac{I_d V_d + I_k V_k}{I_b} \backsimeq \frac{I_d V_d}{I_b} = \frac{P_d}{I_b}, \tag{1}$$

called the discharge loss or the specific discharge power, that has units of watts per ampere [W/A] or electron-volts per ion [eV/ion]. The keeper power is normally small compared with the discharge power and it can be neglected. Since this term represents a power loss, it is desirable to minimize it while maintaining high propellant utilization. The plot of discharge loss versus the propellant utilization efficiency, known as the performance curve, usually characterises the discharge chamber performance of an ion thruster.

Several discharge chamber models, ranging from simple 0-D approach based on power and particle balance to more complicated 2-/3-D multiphysics models, have been developed in the past contributing to a better knowledge of the modelling object and of the impact of the thruster characteristics on its performance. In this analysis, it was decided to use Brophy's model [14] for the ring-cusp and for the Kaufman systems, and Goebel's model [5] for the RF thruster to evaluate the discharge loss as a function of the propellant utilization efficiency because their relative simplicity and accuracy fit the scope of this analytical comparison.

In the following subsections, these models will be described highlighting their peculiarities and differences.

A. 0-D Model for Electron Bombardment (Ring-Cusp and Kaufman) Thrusters

Brophy's model was the first comprehensive analytical discharge chamber model based on particle, charge, and energy balance in the chamber. A uniform plasma (e.g. uniform species densities) and volume-averaged ionization and excitation rates (i.e. average of the ion production and loss) were used in this model and, therefore, it can be considered a 0-dimensional (0-D) model. It was initially developed to describe the performance of a ring-cusped magnetic field, high flux density electron bombardment thruster, but, as suggested by Brophy [3], it can be applied to Kaufman-type thrusters as well with appropriate modifications and considerations to account for the different electron loss mechanism between the two thruster designs: in the ring-cusp configuration, the electrons reach the anode at the cusp points by going along the magnetic field lanes; instead, in the Kaufman type design, the electrons can only reach the anode surface by cross-field diffusion.

In his model, Brophy computes the engine performance as a function of 4 configuration/propellant parameters (the primary electron utilization factor function of the primary electron confinement length, the baseline ion energy cost, the extracted ion fraction, and the cathode potential surface ion fraction) and 2 operating parameters (the propellant flow rate and the discharge voltage).

According to this model, the discharge loss can be written as:

$$\eta_d = \frac{\epsilon_P^*}{f_B\{1-\exp[-C_0 \dot{m}(1-\eta_m)]\}} + \frac{f_C}{f_B} V_d \tag{2}$$

where

$$C_0 = \frac{4\sigma_0 l_c}{e v_0 A_g \phi_0} \tag{3}$$

and

$$\epsilon_P^* = \frac{\epsilon_0^* + \epsilon_M}{1-\left[\frac{V_C+\epsilon_M}{V_d}\right]} \tag{4}$$

The quantity C_0, called the primary electron utilization factor, describes the interaction between primary electrons and neutral atoms and it depends on the primary electron containment length (l_c), the propellant gas (through σ_0, the

total inelastic collision cross section for primary electron-neutral atom collisions, and v_0, the neutral atom velocity), and the quality of the containment of neutrals (through A_g, grid area, ϕ_0, grid transparency to neutral atoms, and v_0).

The quantity ϵ_P^*, called the baseline ion energy cost, is related to different energy loss mechanisms such as: the energy cost expended in excitation compared to ionization of neutral atoms through ϵ_0^*, the average energy of Maxwellian electrons leaving the plasma at the anode ϵ_M, the cathode efficiency V_C that represents an additional potential drop from the hollow cathode insert to where the electrons enter the discharge chamber (e.g. for thrusters with a baffle assembly, V_C is the potential difference between the cathode exit and the exit of the baffle annulus region, through which the electrons are accelerated).

The other parameters present in Eq. (2) are: $f_B = \frac{I_b}{I_P}$ the extracted-ion fraction, and $f_C = \frac{I_c}{I_P}$ the fraction of ion current produces that goes to cathode potential surfaces, where $I_P = en_0 n_e \langle \sigma_+ v_e \rangle V_P$ is the ion production current, where n_0 and n_e are neutral density and plasma density, respectively, $\langle \sigma_+ v_e \rangle$ represents the product of the ionization collision cross section and the electron velocity averaged over the electron speed distribution, and V_P is the plasma volume.

One of the shortcomings of this model is that, since it does not track the path of primary electrons, it cannot consequently predict the primary electron confinement length, and this value needs to be obtained experimentally (or computationally) as well as the extracted-ion fraction.

B. 0-D Model for RF Discharge Thrusters

The ion and electron confinement in RF thrusters is very different than that found in ring-cusp and Kaufman thrusters, hence the models developed for those plasma generators are not directly applicable. Goebel [5] modified his original 0-D ring-cusp model [4] to address these differences, such as the absence of an applied magnetic field that normally confines the plasma particles, and the presence of only Maxwellian electrons inside the chamber.

According to this model, the discharge loss is given by:

$$\eta_d = \frac{P_{abs}}{I_b} \tag{5}$$

The power absorbed by the plasma, P_{abs}, is given by:

$$P_{abs} = I^+ U^+ + I^{++} U^{++} + I^* U^* + (I_s + I_w + I_b)\left(\frac{T_{eV}}{2} + \phi\right) + I_a(2T_{eV} + \phi) \tag{6}$$

where U^+, U^{++}, and U^* are, respectively, the first ionisation potential, the second ionisation potential, and the average excitation potential over the excited species; and I^+, I^{++}, and I^* are, respectively, the singly ionized particle production current, the doubly ionized particle production current, and the excited neutral production current. These potential values are specific for each type of propellant used to generate the plasma. The remaining terms in Eq. (6) are: I_s is the current collected by the screen grid, I_w and I_a are, respectively, the ion and the electron current to the discharge chamber wall, I_b is the beam current, T_{eV} is the electron temperature, and ϕ is the potential of the plasma in the discharge chamber.

Combining the above equations and with some recombination, the discharge loss for RF ion thrusters can be written as:

$$\eta_d = \frac{2n_0 V_P}{v_a A_g T_s}\left(\langle \sigma_i^+ v_e \rangle U^+ + \langle \sigma_i^{++} v_e \rangle U^{++} + \langle \sigma^* v_e \rangle U^*\right) + \left[\frac{1-T_s}{T_s} + \frac{A_w f_{conf}}{A_g T_s} + 1\right](2.5T_{eV} + \phi) \tag{7}$$

The new terms in Eq. (7) are: n_0 is the neutral density; V_P is the plasma volume; v_a is the ion acoustic velocity; A_g and A_w are the grid and wall area, respectively; σ_i^+, σ_i^{++}, and σ^* are the first ionization, the second ionization, and the excitation cross section of the propellant; v_e is the electron velocity; the bracketed term $\langle \quad \rangle$ is called the reaction rate coefficient and consists of the respective cross section averaged over the electron velocity distribution; f_{conf} is the confinement factor defined as the ion current that reaches the wall divided by the Bohm current.

This equation allows to produce the performance curves for different thruster configurations and operating points, requiring as inputs only the geometrical configuration, the grid transparency from an ion optic code, and the electrical input to the discharge chamber. In addition, it allows to calculate the neutral gas pressure, electron temperature, and plasma potential for each configuration.

V. Simulation Results

MATLAB codes based on these models have been written in order to compare the discharge loss of three different thrusters running with different propellants. The three thrusters used as a reference are the QinetiQ T5 (Kaufman-type), the Hughes XIPS13 (ring-cusp type), and the ArianeGroup RIT10-EVO (RF-type). These thrusters have been chosen because they are within the same performance range allowing a more direct comparison. The results of the discharge loss calculations are presented in the following sections. Initially, the codes have been validated for xenon with respect to existing thrusters' experimental data. Following this validation, the parts of the codes depending on the properties of the propellant (e.g., atomic mass, collision cross sections, reaction rates) have been replaced with the values for krypton. Furthermore, it is worth to highlight that the results for the mixture are obtain by interpolating the results of the pure gases using simple arithmetic average.

C. Simulation Results for Kaufman Ion Thrusters

As described in Section IV, the values for l_c, f_B and f_C cannot be predicted using Brophy's model, and experimental data are required. However, such data are not available for the T5 Kaufman thruster, and the following values were assumed for the calculation:

- Primary electron confinement length $l_c = 3\ m$,
- Extracted ion fraction $f_B = 0.4$,
- Fraction of ion current to ion surfaces $f_C = 0.1$.

These values represent a reasonable assumption based on data present in literature [3], and, using these values, the model gives an output of $\eta_d = 292.9\ W/A$ at $\eta_m = 0.87$ for xenon, which is in good agreement with figures present in literature ($\eta_d = 285.6\ W/A$ at $\eta_m = 0.866$) [15].
For validation and comparison purposes, three operating conditions have been considered since available as published data [15] with a particular focus on the 25mN-thrust, and the relative operating points for xenon are reported in Table 1. The result of the simulation for krypton are shown in Figure 4 as performance curves.

Table 1 T5 thruster's operating points [16] **(Xe values) and model results (Kr values)**

Thruster	***T5 (10-cm grid diameter)***		
Nominal thrust T (mN)		25	
Propellant	Xenon	Krypton	1:4 Xe/Kr
Beam voltage V_b (V)		1100	
Beam current I_b (mA)	457	572	542
Propellant mass flow rate $\dot{m}_p$ (mg/s)	0.681	0.592	0.624
Thrust Correction Factor (TCF) γ		0.948	
Specific impulse Isp (s)	3550	4088	3875
Thruster mass utilization efficiency η_m	0.866	0.84	0.84
Discharge loss η_d (W/A)	286	292.4	291
Total power P_{tot} (W)	658	817 (↑24.8%)	779 (↑18.4%)
Power-to-thrust ratio $\frac{P_{tot}}{T_{corr}}$ (W/mN)	27.8	34.6	32.9
Total efficiency η_{tot}	0.627	0.578	0.578

Performance curves allow to characterise the discharge chamber behaviour comparing an output of the thruster to one or more controlled inputs (usually, the discharge loss over a span of mass utilization efficiencies with a set beam current and discharge voltage). Thrusters are usually operated near the "knee" of their performance curve in order to achieve high propellant utilization efficiency without excessive discharge loss. In fact, low discharge loss increases the electrical efficiency of the thruster, and high mass utilization increases its fuel efficiency. The curves shown in Figure 4 were obtained keeping constant the parameters dependent on the thruster design and operational points, such as thruster geometry (A_g, ϕ_0, and l_c), V_d, V_C, f_B, f_C, and varying those dependent on the propellant, such as $\dot{m}_p$, σ_0

and v_0; it was demonstrated in literature [3] that these assumptions are acceptable for testing different propellants while keeping the same thruster. In particular, l_c can be kept constant because it depends on the magnetic field topology (which primarily affects the electrons and not the ions) that, in this analysis, was assumed to be unchanged for the different propellants at each operating point. As result, these performance curves are qualitatively and quantitatively in good agreement with those present in the literature [3], [17], keeping in mind the variations due to different thrusters and operational points.

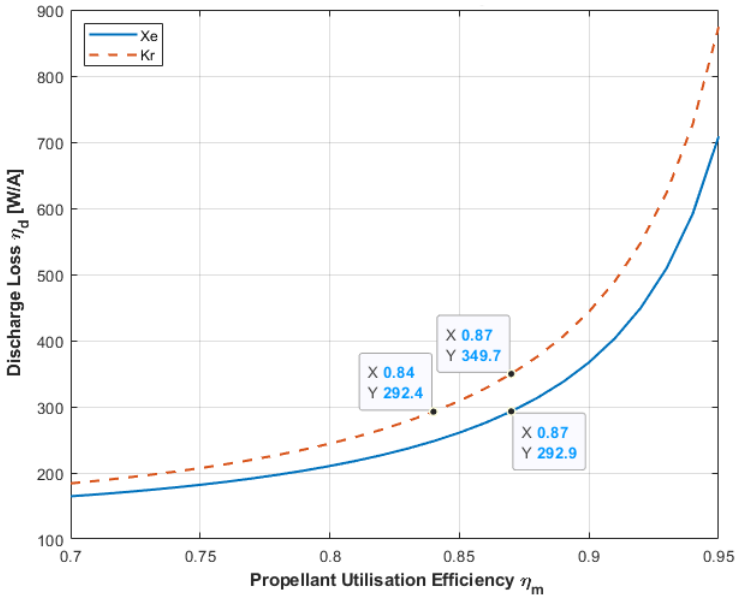

Figure 4 Discharge loss as function of propellant utilization efficiency for T5 thruster at T=25 mN

The resulting performance data for krypton are reported in Table 1 and they give a reference on the order of magnitude of the penalties in performance when krypton is used. If the selected operational points for krypton were chosen with the intention to limit the discharge loss (i.e. comparable to the value obtained with xenon, with the consequence of a lower propellant utilization efficiency), the power penalties in this case would be of around 25% and around 18% for the mixture to obtain the same thrust. In this case, when running the thruster with krypton at the same utilization efficiency as xenon, the total power increase is around 30% and around 22% for the mixture.

However, previously published data [18] suggest that higher discharge voltage values are beneficial (and sometimes necessary) when using krypton. In Figure 5, the relative change in discharge loss for three different discharge voltages while keeping the beam current constant (457 mA for xenon and 572 mA for krypton) is shown: in fact, this suggestion is confirmed by the result of the calculation as the gap in performance between xenon and krypton is reduced when V_d is increased. This behaviour is due to krypton's higher ionization and excitation potentials and relative reaction rates compared to xenon since an increase in V_d increases the primary electrons energy and, consequently, the ionization rate. However, operating the thruster at higher discharge voltages can introduces issues related to an increased erosion of the cathode surfaces in the discharge chamber due to higher-energy ion sputtering [18].

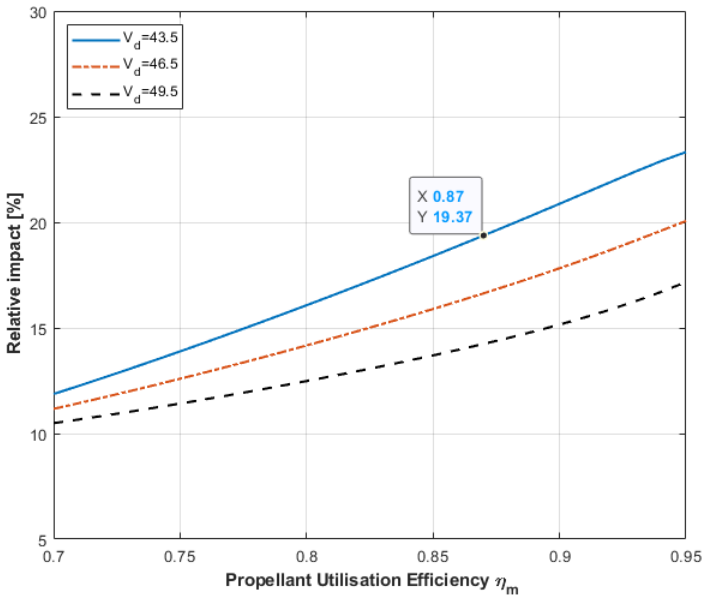

Figure 5 Relative change in discharge loss from xenon to krypton for different V_d

D. Simulation Results for Ring-Cusp Ion Thrusters

A similar approach has been used to calculate the impact of using krypton with the XIPS13 ring-cusp thruster. However, in this case, the values for l_c, f_B and f_C are available in literature [19]:

- Primary electron confinement length $l_c = 4.16\ m$,
- Extracted ion fraction $f_B = 0.3$,
- Fraction of ion current to ion surfaces $f_C = 0.1$.

Using these values, the model gives as an output $\eta_d = 251.9\ W/A$ at $\eta_m = 0.82$ for xenon that is in good agreement with the one present in literature ($\eta_d = 250.4\ W/A$ at $\eta_m = 0.818$)[20].

In this case, a single operating condition is available in literature [20] and its operating points are reported in Table 2 for xenon. In Figure 6, the result of the simulation for krypton are shown as performance curve and the selected operating point is reported in Table 2.

Table 2 XIPS13 thruster's operating point [48] (Xe values) and model results (Kr values)

Thruster	*XIPS13 (13-cm grid diameter)*		
Nominal thrust T (mN)		18	
Propellant	Xenon	Krypton	1:4 Xe/Kr
Beam voltage V_b (V)		750	
Beam current I_b (mA)	405	507	480
Propellant mass flow rate $\dot{m}_p$ (mg/s)	0.655	0.572	0.603
Thrust Correction Factor (TCF) γ		0.973	
Specific impulse Isp (s)	2771	3176	3010
Thruster mass utilisation efficiency η_m	0.818	0.77	0.77
Discharge loss η_d (W/A)	250.4	252.2	251.8
Total power P_{tot} (W)	438.5	541 (↑23.5%)	515 (↑17.4%)
Power-to-thrust ratio $\frac{P_{tot}}{T_{corr}}$ (W/mN)	24.6	30.4	28.9
Total efficiency η_{tot}	0.551	0.512	0.510

Similar to the Kaufman case, the selected point for krypton gives a discharge loss value comparable to the value with xenon, and the resulting total power increase is around 23.5% and around 17.4% for the mixture. As a reference, this value would increase to 30% when running the thruster with krypton at the same utilisation efficiency as xenon, and around 22% for the mixture.

Furthermore, the calculation of the relative change in discharge loss for three different discharge voltages while keeping the beam current constant (405 mA for xenon and 507 mA for krypton) has been carried out and the results are shown in Figure 7. It is again confirmed that increasing the discharge voltage decreased the difference in discharge loss between xenon and krypton.

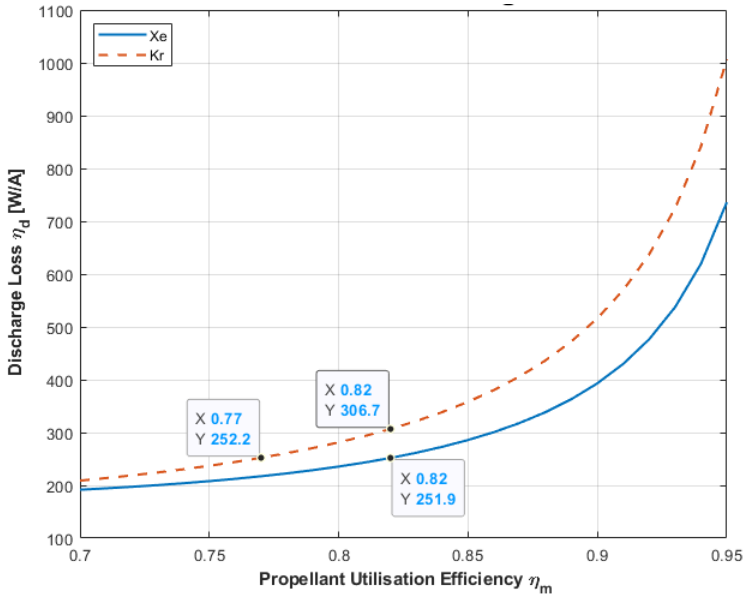

Figure 6 Performance curve for XIPS13 thruster at T=18 mN

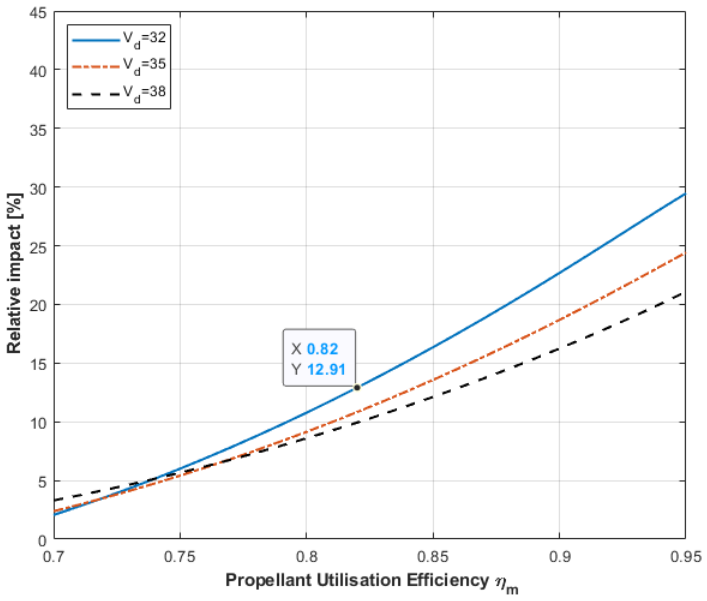

Figure 7 Relative change in discharge loss from xenon to krypton for different V_d

E. Simulation Results for RF Ion Thrusters

As previously mentioned, the self-consistent Goebel's model [5] has been used for the RF thruster case. A direct consequence is that the performance curves can be obtained from the required inputs (i.e. geometry, ion optics, and electrical inputs) without the need for experimental inputs. However, it is worth to highlight that the modelling of the induced magnetic field and of the confinement factor is of fundamental importance in determining the discharge loss.

Based on the data available in literature [21], the calculated magnetic field is equal to $16.872\,G$, and the corresponding confinement factor are equal to 0.4476 for xenon and 0.38 for krypton. Using these values, the model output is $\eta_d = 354.2\,W/A$ at $\eta_m = 0.86$ for xenon that is in good agreement with the one present in literature ($\eta_d = 352\,W/A$ at $\eta_m = 0.856$) [22].

A single operating condition is available in literature [22] and its operating points are reported in Table 3 for xenon. In Figure 8, the result of the simulation for krypton are shown as performance curve and the selected operating point is reported in Table 3.

Table 3 RIT10-EVO thruster's operating point [21] (Xe values) and model results (Kr values)

Thruster	*RIT10-EVO (9-cm grid diameter)*		
Nominal thrust T (mN)	25		
Propellant	Xenon	Krypton	1:4 Xe/Kr
Beam voltage V_b (V)	1230		
Beam current I_b (mA)	444	556	527
Propellant mass flow rate $\dot{m}_p$ (mg/s)	0.692	0.603	0.637
Thrust Correction Factor (TCF) γ	0.98		
Specific impulse Isp (s)	3711	4256	4034
Thruster mass utilisation efficiency η_m	0.856	0.8	0.8
Discharge loss η_d (W/A)	352	355	354
Total power P_{tot} (W)	715.7	898 (↑25.4%)	850 (↑18.8%)
Power-to-thrust ratio $\frac{P_{tot}}{T_{corr}}$ (W/mN)	28.4	35.7	33.8
Total efficiency η_{tot}	0.640	0.585	0.585

Like in the previous two cases, the results for krypton have been obtained by varying only the parameters related to the propellant and keeping all the others constant. The increase in absorbed power is equal to 25.4% for the selected point (i.e. similar discharge loss for xenon and krypton) for krypton and around 18.8% for the mixture, while it would be equal to 28.3% for similar propellant utilisation efficiency, and around 21% for the mixture.

In the RF thruster case, there are not any available data in literature that would suggest a better operating mode for running the thruster with krypton, and since this type of thrusters work without any discharge electrodes, it is not possible to increase the discharge voltage to reduce the gap in performance between xenon and krypton.

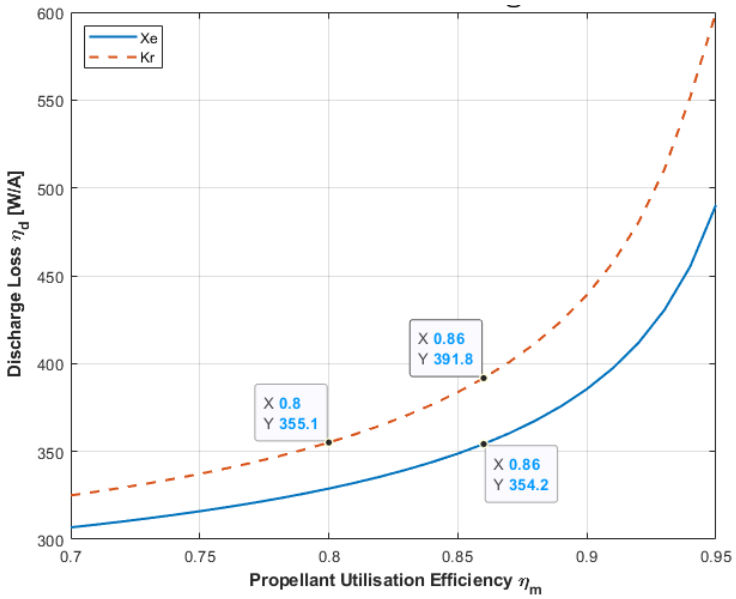

Figure 8 Performance curve for RIT10-EVO thruster at T=25 mN

F. Summary on Performance Models' Results

0-D models have been used to evaluate the impact of using krypton instead of xenon for three different types of GIE plasma generator. The result of the comparison shows that the three thrusters provide a similar behaviour and similar loss in performance when alternative propellants are used. In fact, the relative increase in total power is around

23.5-25.5% for krypton and around 17-19% for the mixture when the operating points' selection is based on keeping similar discharge loss for the three propellants, and it goes up to 28-30% for krypton and to 21-22% for the mixture if the operating points are chosen based on maintaining the same propellant utilisation efficiency. A plausible explanation of this similarity in the impact of changing propellant is that the global models used for the calculations represent the plasma as uniform in the discharge chamber and the plasma properties (i.e. temperatures, densities, etc.) are constant and averaged over the volume of the chamber. Consequently, the main difference within each model is related to propellant-specific properties (i.e. ionisation and excitation potentials, and respective reaction rates) which are uniform for the three models.

VI. Conclusion

The analysis of the impact of using krypton and a 1:4 Xe/Kr mixture on the discharge chamber performance has been carried out for three different plasma generators using 0-D models with the objective to quantify and, possibly, identify the technology least impacted by the change of propellant. The calculation has assessed that using krypton instead of xenon would require an increase of total input power in the range of 23 to 30% depending on the selected operating points. In addition, it was shown that no plasma generators offer a clear advantage over the competing technologies.

Acknowledgments

The authors would like to thank the University of Southampton for the support. This research has been funded by the European Commission in the scope of the GIESEPP project, within the frame of the H2020 Research program - COMPET-3-2016-a SRC - In-Space Electrical Propulsion and Station Keeping, Incremental Line - Gridded Ion Engines of the European Union (Research and Innovation contract No.730002).

References

[1] F. Infed *et al.*, "Gridded Ion Engine Standardised Electric Propulsion Platforms," 2017.

[2] N. Fazio, S. B. Gabriel, and I. O. Golosnoy, "Alternative Propellants for Gridded Ion Engines," in *6th Space Propulsion Conference*, 2018, pp. 1–8.

[3] J. R. Brophy and P. J. Wilbur, "Ion Thruster Performance Model," Colorado State University, Fort Collins, Colorado, USA, 1984.

[4] D. M. Goebel, R. E. Wirz, and I. Katz, "Analytical Ion Thruster Discharge Performance Model," *J. Propuls. Power*, vol. 23, no. 5, pp. 1055–1067, Sep. 2007, doi: 10.2514/1.26404.

[5] D. M. Goebel, "Analytical Discharge Model for RF Ion Thrusters," *IEEE Trans. Plasma Sci.*, vol. 36, no. 5 PART 1, pp. 2111–2121, 2008, doi: 10.1109/TPS.2008.2004232.

[6] N. Fazio, S. B. Gabriel, I. O. Golosnoy, and B. Wollenhaupt, "Mission Cost for Gridded Ion Engines using Alternative Propellants," in *36th International Electric Propulsion Conference*, 2019, pp. 1–21, [Online]. Available: https://eprints.soton.ac.uk/434549/.

[7] C. M. Simon, R. Mercado, S. K. Schnell, B. Smit, and M. Haranczyk, "What Are the Best Materials To Separate a Xenon/Krypton Mixture?," *Chem. Mater.*, vol. 27, no. 12, pp. 4459–4475, Jun. 2015, doi: 10.1021/acs.chemmater.5b01475.

[8] D. M. Goebel and I. Katz, *Fundamentals of Electric Propulsion: Ion and Hall Thrusters*, 1st ed. Hoboken, New Jersey, USA: John Wiley & Sons, 2008.

[9] H. W. Loeb, "Plasma-based ion beam sources," *Plasma Phys. Control. Fusion*, vol. 47, no. 12B, pp. B565–B576, 2005, doi: 10.1088/0741-3335/47/12b/s41.

[10] M. S. Hutchins, H. B. Simpson, and J. J. Palencia, "QinetiQ's T6 and T5 Ion Thruster Electric Propulsion System Architectures and Performances," 2015.

[11] D. A. Herman and A. D. Gallimore, "Discharge Chamber Plasma Structure of a 40-cm NEXT-type Ion Engine," in *41st AIAA/ASME/SAE/ASEE Joint Propulsion Conference & Exhibit*, 2005, p. 4250.

[12] QinetiQ, "Gridded Ion Engines [PowerPoint slides]." EPIC Lecture Series 2017, 2017, [Online]. Available: http://epic-src.eu/wp-content/uploads/06_EPICLectureSeries2017_QinetiQ_GIE_EPIC-Lecture-Series-2017.pdf.

[13] H. J. Leiter *et al.*, "Evolution of the AIRBUS DS GmbH Radio Frequency Ion Thruster Family," 2015.

[14] J. R. Brophy and P. J. Wilbur, "Simple Performance Model for Ring and Line Cusp Ion Thrusters," *AIAA J.*, vol. 23, no. 11, pp. 1731–1736, Nov. 1985, doi: 10.2514/3.9158.

[15] M. W. Crofton, "Evaluation of the United Kingdom Ion Thruster," *J. Spacecr. Rockets*, vol. 33, no. 5, pp. 739–747, 1996, doi: 10.2514/3.26829.

[16] M. W. Crofton, "Evaluation of the T5 (UK-10) Ion Thruster: Summary of Principal Results," 1995.

[17] J. S. Sovey, "Improved Ion Containment using a Ring-Cusp Ion Thruster," *J. Spacecr. Rockets*, vol. 21, no. 5, pp. 488–495, Sep. 1984, doi: 10.2514/3.25684.

[18] M. J. Patterson and J. G. J. Williams, "Krypton Ion Thruster Performance," 1992, doi: 10.2514/6.1992-3144.

[19] E. R. Torres and M. Martinez-Sanchez, “Prediction of the Performance of an Ion Thruster Using Buckminsterfullerene as Propellant,” Massachusetts Institute of Technology, Cambridge, Massachusetts, USA, 1993.
[20] J. R. Beattie, J. D. Williams, and R. R. Robson, “Flight qualification of an 18-mN xenon ion thruster,” in *23rd AIAA/AIDAA/DGLR/JSASS International Electric Propulsion Conference*, 1993, pp. 93–106.
[21] H. W. Loeb, K.-H. Schartner, S. Weis, D. Feili, and B. K. Meyer, “Development of a RIT-Millithruster,” in *55th International Astronautical Congress of the International Astronautical Federation, the International Academy of Astronautics, and the International Institute of Space Law*, Oct. 2004, pp. 1–9, doi: 10.2514/6.IAC-04-S.4.04.
[22] H. Bassner, R. Killinger, H. J. Leiter, and J. Mueller, “Advantages and Applications of the RF-Ion Thruster BIT,” 2001, doi: doi:10.2514/6.2001-3494 10.2514/6.2001-3494.